ARTICLE

One-Step Photoembossing for Submicrometer Surface Relief Structures in Liquid Crystal Semiconductors

Alicia Liedtke,[†] Chunhong Lei,[†] Mary O'Neill,[†,*] Peter E. Dyer,[†] Stuart P. Kitney,[‡] and Stephen M. Kelly[‡]

[†]Department of Physics and [‡]Department of Chemistry, University of Hull, Cottingham Road, Hull, HU6 7RX, U.K.

ABSTRACT We report a new single-step method to directly imprint nanometer-scale structures on photoreactive organic semiconductors. A surface relief grating is spontaneously formed when a light-emitting, liquid crystalline, and semiconducting thin film is irradiated by patterned light generated using a phase mask. Grating formation requires no postannealing nor wet etching so there is potential for high-throughput fabrication. The structured film is cross-linked for robustness. Gratings deeper than the original film thickness are made with periods as small as 265 nm. Grating formation is attributed to mass transfer, enhanced by self-assembly, from dark to illuminated regions. A photovoltaic device incorporating the grating is discussed.

KEYWORDS: molecular electronics · liquid crystals · photonics · nanoimprinting · organic photovoltaics · self-assembly · photolithography

The nanoscale patterning of the surfaces of organic semiconductors is a relatively young research area. Current applications include the provision of distributed feedback in organic lasers,[1,2] enhanced efficiency from OLEDs with corrugated structures,[3] and the formation of channel waveguides.[4] The enormous potential of this technology can be understood by analogy with inorganic semiconductors where more sophisticated patterned thin films have been used to slow light down[5] and to develop photonic bandgap waveguides for optical communications.[6] A key factor in delivering the potential of patterned semiconductors is the development of low-cost large-area patterning techniques.[7] Embossing and nanoimprinting techniques are often used to pattern the surface features on organic semiconductors.[8−10] Patterns are created by mechanical deformation of the organic thin film using a mold with topographic features. Very good resolution is obtained but the masters are expensive. The process relies on displacing polymer in confined spaces, which may lead to systematic errors for large-area patterning. Hard contact with the stamp may also be detrimental to the yield of devices. The photolithographic patterning of photopolymerizable organic semiconductors involves a wet etching step to develop the structures.[11,12] Laser ablation is also used[13] but is incompatible with high-through-put manufacturing. We now report a new single-step photoembossing method to directly imprint nanometer-scale structures on organic semiconductors. A surface relief grating is spontaneously generated on irradiation of a photopolymerizable, light-emitting, liquid crystalline, semiconducting thin film through a phase mask. No postannealing or wet etching step is required bringing the potential for high-through-put fabrication.

Photoembossed surface relief structures have been formed in nonsemiconducting photopolymers and nematic monomers used for holography by irradiation with spatially modulated UV light.[14−19] The free radicals created in the illuminated areas are captured in the glassy matrix, but monomer diffusion to the reactive sites is usually restricted until a development stage where the sample is heated above a threshold temperature and the sample changes to a more mobile, liquid-like state. Spatial gradients in the chemical potential provide a driving force for the monomers to diffuse from the unexposed to the exposed areas, creating a volume increase in the latter region and consequently a surface relief structure. Surface structures can also be reversibly formed in nonsemiconducting, but photoactive, materials containing azobenzene or other photoisomerizable groups,[20,21] where the doping with liquid crystals enhances grating formation.[22] The formation of gratings has also some unusual polarization effects; large amplitudes are obtained by interference of two orthogonal circularly polarized beams even

*Address correspondence to m.oneill@hull.ac.uk.

Received for review January 4, 2010 and accepted April 28, 2010.

Published online May 10, 2010. 10.1021/nn100012g

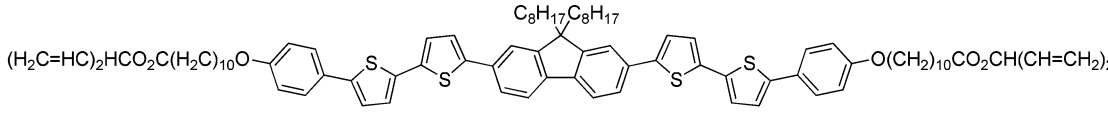

Compound **1**

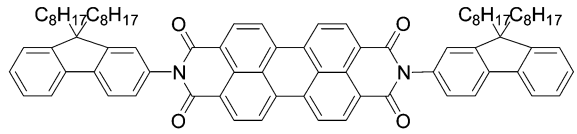

Compound **2**

Figure 1. Chemical structures and transition temperatures of compounds 1 and 2. Compound 1: T_g = 0°; Cr, 52 °C; N, 143 °C. Compound 2: Cr−I = 274 °C (glass forms on rapid quenching in thin films).

though there is no intensity modulation. Several mechanisms for photoinduced mass migration of azobenzene molecules have been suggested, for example, the gradient force of the optical electric field, isomerization-driven free volume expansion, and the mean field theory of anisotropic intermolecular interaction, *etc.* Indeed an azo-containing polymer was deposited on top of a dye-doped organic gain media to provide feedback in a distributed feedback laser.[23] The azo-group quenched luminescence and so could not be incorporated into the gain medium.

RESULTS AND DISCUSSION

Figure 1 shows the chemical structure of the organic semiconductor **1** used for the photoembossing studies and its phase transition temperatures. It is a liquid crystalline monomer consisting of a light-emitting/charge-transporting aromatic core between two flexible spacers each incorporating a photopolymerizable nonconjugated diene.[24] Although the glass transition temperature is below room temperature, thin films of **1** retain a glassy nematic state for long periods at room temperature on quenching from the nematic phase. **1** is hole-transporting with a mobility of 2×10^{-5} cm^2 V^{-1} s^{-1} at room temperature.[25] A similar reactive mesogen with an extended aromatic core has a mobility $>3 \times 10^{-3}$ cm^2 V^{-1} s^{-1}.[26] **1** emits green light peaking at a wavelength of 510 nm with a solid-state photoluminescence quantum efficiency of 27%. An OLED incorporating **1** produced 380 cd m^{-2} at a voltage of 5 V with an efficacy of 1.6 cd A^{-1}.[12,27] Semiconducting reactive mesogens have been used to produce a red, green, and blue pixellated OLED and organic photovolatics with distributed interfaces to improve charge separation.[12,28] OLED efficacies up to 6.8 cd A^{-1} are obtained.[29]

Surface relief gratings are spontaneously formed by irradiating 80 nm thin films of **1** on a glass substrate at 65 °C or room temperature with collimated light from a HeCd laser of wavelength 325 nm transmitted through a phase mask at normal incidence. The transmitted light for an ideal zero-order suppressed phase mask has components at the ± 1 diffraction orders only, giving an interference pattern of period $\Lambda/2$. The interference field produced by the phase mask used in the experiment was analyzed, taking into account the polarization of the laser and the incomplete zero-order suppression.[30] The laser had sufficiently large temporal coherence that its emission could be assumed to be monochromatic. Calculations included finite spatial coherence to account for the presence of multiple transverse modes (source angular size = 1 mrad). In the $E_\parallel$ configuration the input electric field is parallel to the grating wave-vector of the phase mask (perpendicular to the grooves), so that the electric field vectors of the diffracted beams are not parallel, which leads to incomplete interference. This is shown in Figure 2 where the irradiance distribution parallel to the phase mask surface ($x-z$ plane) for the $E_\parallel$ mode consists of a high background on which is superimposed a set of peaks and troughs, which vary periodically with distance (y) from the phase mask. The distances in Figure 2 are normalized to Λ. The irradiance distribution has a period of Λ along x, when y is equal to zero and 1.5, but in the latter case the peaks are shifted laterally by 0.5 Λ. Between these two distances the distribution is double peaked along x and the period becomes $\Lambda/2$ when the irradiance of the two peaks become equal.

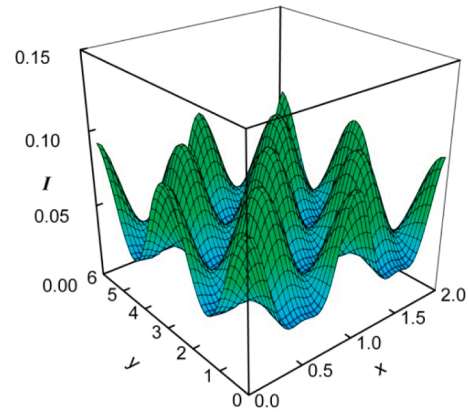

Figure 2. Calculated irradiance distribution *I* (arbitrary units) for laser radiation of wavelength 325 nm transmitted through the phase mask of period Λ = 530 nm. The incident beam has $E_\parallel$ polarization. The mask surface lies in the $x-z$ plane with the grooves oriented along z. Distances along x (parallel to the mask surface, and y (perpendicular to the mask surface) are normalized to Λ.

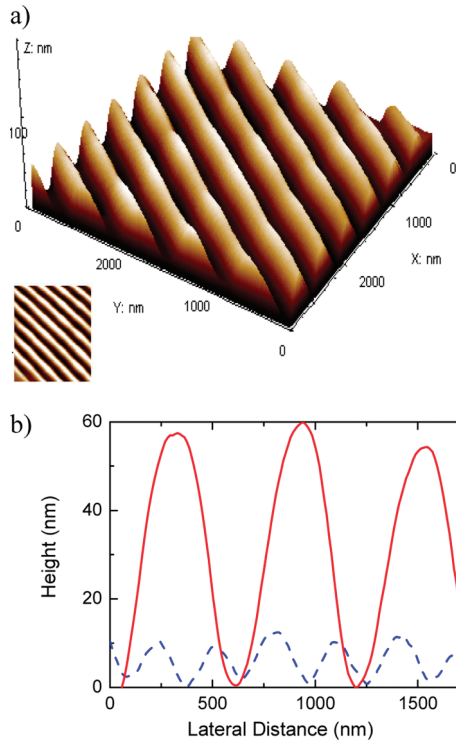

Figure 3. (a) AFM topology of a surface relief grating produced by irradiating a thin film of 1 with $E_{\parallel}$ polarized radiation at 65 °C transmitted through the 530 nm period phase mask. (b) Surface profile (solid line) derived from panel a and that from another sample (dashed line) irradiated using similar conditions but with $E_{\perp}$ polarization.

Hence, the period of the photoembossed gratings is expected to be very sensitive to the phase mask-sample separation. In the $E_{\perp}$ configuration, the electric field component of the incident beam is perpendicular to the grating vector of the phase mask (parallel to the grooves). The polarization vectors of the diffracted beams are also parallel so high contrast interference fringes are obtained, as shown in supporting Figure 1. Figure 3a shows an atomic force microscopy (AFM) image of a surface relief grating on a thin film of **1** produced by irradiation through a 530 nm phase mask in the $E_{\parallel}$ configuration. A period of 580 nm is found, which is within 10% of Λ. Figure 3b shows a cross-section of the surface profile obtained and that from another sample irradiated using similar conditions but in the $E_{\perp}$ configuration. In the latter case a shallower grating is found with a period of 285 nm, approximately equal to $\Lambda/2$. Double-peaked gratings were obtained at other times. These results suggest that the corrugation profile reflects the irradiance distribution at the surface of the sample. The irradiance distribution has a low contrast between the peaks and troughs when the period is $\Lambda/2$, which may explain the shallower grating obtained for these conditions. The deviation of the grating period from exactly $\Lambda/2$ or Λ cannot be explained by tilting of the sample and requires further investigation. Irradiation of the sample using a 1 μm phase mask produced gratings with periods approximately equal

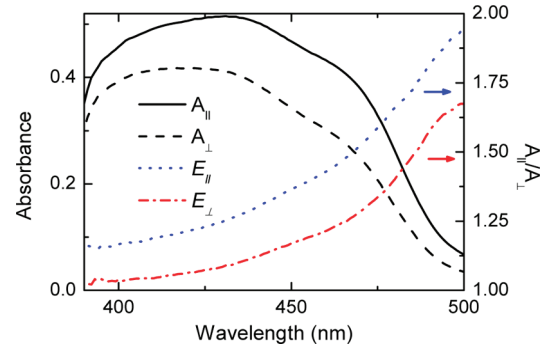

Figure 4. Absorbance spectrum of a sample of 1 measured with a probe beam polarized parallel (∥) and perpendicular (⊥) to the wave-vector of the photoembossed grating. The grating was photoembossed using the $E_{\parallel}$ configuration. The polarization ratio ($A_{\parallel}/A_{\perp}$) is shown as a function of wavelength for both the $E_{\parallel}$ and $E_{\perp}$ photoembossing configurations as labeled.

to Λ. This phase mask had poor zero-order suppression so no structures of period $\Lambda/2$ were obtained. In general, the depth of the gratings varied with the grating period. Depths up to 140 nm were obtained using the 1 μm phase mask at 65 °C. For the 530 nm phase mask, gratings of amplitude 66 and 25 nm were found for periods of about Λ and $\Lambda/2$, respectively. The grating amplitudes were smaller at room temperature. The grating structures formed are uniform over small areas as shown in Figure 3a, but become nonuniform over large areas because of sample tilt misalignment. Modeling shows that this technical problem would be avoided by improved zero-order suppression of the phase mask so that the distance in the *y* direction over which the fringes become displaced laterally becomes longer. Alternatively a holographic setup could provide high contrast uniform optical fringes over large areas.

The depth of some gratings is larger than the thickness of the original film. As the irradiance of the continuous wave HeCd laser is too low to cause ablation, this suggests that their formation involves mass transfer, as discussed for other materials above. We propose that the polymerization-induced change of chemical potential drives mass transfer from regions where there are troughs in irradiance toward the regions containing peaks. The contrast in irradiance between the peaks and troughs of the simulated light distribution is small so that photopolymerization occurs over the whole irradiated region, but at varying rates, which is expected to limit the maximum grating amplitude obtained.

Surprisingly the gratings were always deeper, by up to a factor of 2, for irradiation using the $E_{\parallel}$ rather than the $E_{\perp}$ configuration, even though the interference has higher contrast for $E_{\perp}$, see above. Photopolymerization is expected to occur sooner in the trough regions in the $E_{\parallel}$ case, thus inhibiting mass transfer and producing shallower gratings. Figure 4 shows the absorption spectra of a photoembossed thin film of **1**, measured using a probe source polarized parallel ($A_{\parallel}$) and perpendicular ($A_{\perp}$) to the grating vector of the photoinduced grating.

The grating was made using the $E_{\parallel}$ configuration, and the polarized absorption indicates that a photoinduced reorientation of the molecules took place during grating formation. The polarization ratio of the absorbance ($A_{\parallel}/A_{\perp}$) is smaller when the grating is embossed using the $E_{\perp}$ configuration, implying a smaller reorientation under conditions where shallower gratings are formed. Anisotropic photopolymerization may explain both phenomena. No photoinitiator is added to the mesogen suggesting that the cross-linking process is self-initiated by the chromophore. The self-initiation does not proceed by fragmentation of the aromatic core and may occur *via* thermally assisted energy transfer from the excited state of the aromatic core to the cross-linking group.[31] Chromophores parallel to the polarization direction of the incident beam are preferentially excited. Assuming a short-range energy transfer to the polymerizable diene group of the excited mesogen, their alignment will be locked in by cross-linking with neighboring monomers. The alignment is enhanced by the cooperative reorientation of nearest neighbors resulting from the self-assembly properties of nematics. The shear viscosity of nematic liquid crystals is anisotropic and is minimized for translation parallel to the director, the preferred alignment direction of the liquid crystal.[32] Hence, monomers lying perpendicular to the grating grooves can flow more easily into the more highly cross-linked regions of the film. These monomers are parallel to the photoinduced alignment direction in the $E_{\parallel}$ case and perpendicular to the preferred alignment of $E_{\perp}$ irradiation. Hence, cooperative effects are greater in the former case leading to greater mass diffusion, deeper gratings, and a larger photoinduced orientation. Similar cooperative effects were observed during mass transport of nonsemiconducting liquid crystals.[19] A photoinduced polarization of similar magnitude is observed in thin films of **1** uniformly cross-linked by a linearly polarized beam at room temperature. This suggests a photoinduced reduction of viscosity,[33] although there may be a thermal contribution from sample heating by the beam. However the latter was minimal since we scanned the beam of absorbed intensity <0.05 W cm^{-2} over the phase mask so that each region was continually exposed only for intervals <10 s. Similar materials with higher transition temperatures[29] did not show photoinduced anisotropy and formed only negligibly shallow grating by photoembossing because of their much higher viscosity.

The photoembossed surface gratings can be successfully incorporated in an optoelectronic device. Charge separation normally occurs in organic photovoltaics at a heterointerface by trapping the hole and electron, respectively, in electron-donating and electron-accepting materials. The electron-accepting layer overlies the electron-donating thin film in bilayer photovoltaics to provide the necessary asymmetry to ensure that electron and holes reach different electrodes.

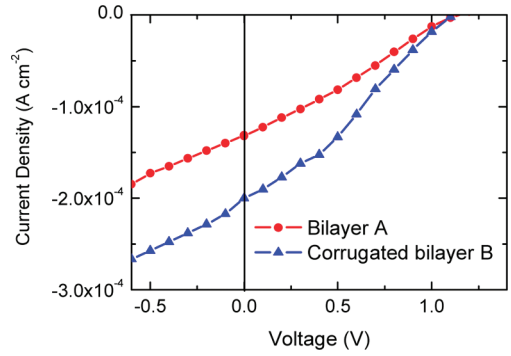

Figure 5. Photocurrent−voltage characteristic of bilayer photovoltaic devices A and B. The input power density was at 24 mW cm^{-2} at 470 nm.

The diffusion length of the exciton before recombination is very short, ~10 nm, so that bilayer devices are necessarily thin to ensure excitons reach the interface before recombination. Compound **1** has a relatively low ionization potential (IP) of ~5.5 eV, so that it used as the electron-donating species in the device. Compound **2**, see Figure 1, is a glassy perylene containing material (*N*,*N*′-bis(9,9-dioctylfluoren-2-yl)perylene-3,4,9,10-tetracarboxyldiimide) whose chemical synthesis is reported elsewhere.[34] It has a high electron affinity (EA) of 4.2 eV, so it forms the electron-accepting layer of the device. The difference between the IP of **1** and the EA of **2** is 1.3 eV, which is smaller than the energy of the absorption band-edge of both materials so that charge separation at the donor−acceptor interface is thermodynamically favorable. Figure 5 shows the current voltage characteristics of two bilayer devices consisting of a thin film of the cross-linked electron-donating material **1** overlaid with the electron-accepting material **2**. The two devices were processed similarly except for the photopolymerization of **1**.

The thin film of **1** was irradiated uniformly for device A and through the 530 nm period phase mask for device B. AFM shows that a surface relief grating of period 265 nm and ~30 nm depth was obtained in device B. A shallower corrugation of <10 nm is found, see Supporting Information, Figure 2, when layer **2** was deposited on top showing that the solution processing of the upper layer does not result in mixing of the layers and destruction of the grating. The photovoltaic devices A and B were found to have a power conversion efficiency of 0.16% and 0.28%, respectively, for the same operating conditions (24 mW cm^{-2} at 470 nm). The significant improvement in performance for the grating device cannot be explained by an increase of the effective interface length by the corrugation as this is calculated to be $<4\%$, assuming a sinusoidal corrugation. However the corrugated interface penetrates about half the depth of the electron donating- and accepting-layers and so provides variable distances between the interface and the collection electrodes. The electron mobility of **2** is very low ($<10^{-5}$ cm^2 V^{-1} s^{-1}), so that space

charge builds up at the interface leading to nonradiative geminate recombination of electron−hole pairs. The improved performance from the corrugated device may result from better collection of the charge from regions where the electrode is more closely spaced. A much smaller grating period approaching the exciton diffusion length would be required to guarantee complete charge separation throughout the bilayer.

CONCLUSION

We have demonstrated the spontaneous and single-step formation of surface nanostructures by mass transfer in thin films of light-emitting, semiconducting, and polymerizable liquid crystals upon irradiation with patterned UV light. The mass transfer is enhanced by co-operative effects when the incident beam is polarized parallel to the grating wave vector. Surface relief gratings of amplitude up to 140 nm have been obtained even though the films were originally only 80 nm deep. The nanostructured film is cross-linked for robustness and environmental stability. Holographic methods would give uniform gratings over large areas and could also be developed to obtain 2D structures with nanocavities. Grating periods as small as 265 nm were achieved, and it has been shown that the gratings can be successfully incorporated in bilayer photovoltaics. The smallest period obtained approaches that required, ~250 nm,[35] to make a second-order-distributed feedback structure for lasing near the emission peak of the material at 510 nm. Hence the photoembossing process has major potential applications in photonics.

EXPERIMENTAL SECTION

Sample preparation and exposure were carried out in a glovebox under nitrogen atmosphere with humidity of less than 1 ppm and an oxygen concentration less than 30 ppm. Glass slides covered with an ~40 nm layer of rubbed polystyrene sulfonate/polyethylene dioxythiophene (PSS/PEDOT) (Baytron P VP AI 4083) were used as substrates. Thin films of **1** were deposited by spin-casting from solution in chlorobenzene (~0.03 mg μL^{-1}). The films were spun at 900 rpm for 30 s and then heated at 65 °C for 15 min. The films were then irradiated with a HeCd laser (325 nm) of irradiance, ~0.4 W cm^{-2}, through a phase mask in close contact with the sample for a total fluence of 600 J/cm^2 either at 65 ± 2 °C or at room temperature. A Picoscan scanning probe microscope from Molecular Imaging was used for the atomic force microscopy (AFM) scans. Photovltaic devices were fabricated on indium tin oxide (ITO) coated glass (13 $\Omega\,\square^{-1}$) substrates. The substrates were first plasma etched and coated with a PSS/PEDOT layer which was baked at 160 °C for 30 min. Subsequently, the electron-donating material **1** was spin-coated from a 1.5 wt % chlorobenzene solution onto the substrates. The films were cross-linked by irradiation with the 325 nm HeCd laser without a mask (device A), or through the 530 nm phase mask in the $E_\perp$ configuration (device B) at 65 °C. Then the electron-accepting material **2** was spin-coated at 2000 rpm from a 1.0 wt % chlorobenzene solution onto the electron-donating layer and annealed at 120 °C for 60 min. A cathode of lithium fluoride (0.6 nm) and aluminum (50 nm) was deposited by evaporation. The current−voltage characteristics of the photovoltaic devices were measured in a nitrogen atmosphere using a visual-basic controlled homemade picoammeter in the dark and on illumination with a xenon lamp, dispersed through a monochromator and atttenuated with neutral density filters.

Acknowledgment. We thank G. Sowersby for technical support and G. Cutler, S. Cutler, and C. Walton for technical advice.

Supporting Information Available: Calculated irradiance distribution for an incident beam with $E_\perp$ polarization (Figure 1); AFM images of a surface relief grating before and after the deposition of an overlying layer (Figure 2). This material is available free of charge *via* the Internet at http://pubs.acs.org.

REFERENCES AND NOTES

1. McGehee, M. D.; Diaz-Garcia, M. A.; Hide, F.; Gupta, R.; Miller, E. K.; Moses, D.; Heeger, A. J. Semiconducting Polymer Distributed Feedback Lasers. *Appl. Phys. Lett.* **1998**, *72*, 1536–1538.
2. Samuel, I. D. W.; Turnbull, G. A. Organic Semiconductor Lasers. *Chem. Rev.* **2007**, *107*, 1272–1295.
3. Ziebarth, J. M.; Saafir, A. K.; Fan, S.; McGehee, M. D. Extracting Light from Polymer Light-Emitting Diodes Using Stamped Bragg Gratings. *Adv. Funct. Mater.* **2004**, *14*, 451–456.
4. Gather, M. C.; Ventsch, F.; Meerholz, K. Embedding Organic Light-Emitting Diodes into Channel Waveguide Structures. *Adv. Mater.* **2008**, *20*, 1966–1971.
5. Baba, T. Slow Light in Photonic Crystals. *Nat. Photon.* **2008**, *2*, 465–473.
6. Noda, S.; Chutinan, A.; Imada, M. Trapping and Emission of Photons by a Single Defect in a Photonic Bandgap Structure. *Nature* **2000**, *407*, 608–610.
7. Menard, E.; Meitl, M. A.; Sun, Y.; Park, J. U.; Shir, D. J. L.; Nam, Y. S.; Jeon, S.; Rogers, J. A. Micro- and Nanopatterning Techniques for Organic Electronic and Optoelectronic Systems. *Chem. Rev.* **2007**, *107*, 1117–1160.
8. Chou, S. Y.; Krauss, P. R.; Renstrom, P. J. Imprint Lithography with 25-Nanometer Resolution. *Science* **1996**, *272*, 85–87.
9. Meier, M.; Dodabalapur, A.; Rogers, J. A.; Slusher, R. E.; Mekis, A.; Timko, A.; Murray, C. A.; Ruel, R.; Nalamasu, O. Emission Characteristics of Two-Dimensional Organic Photonic Crystal Lasers Fabricated by Replica Molding. *J. Appl. Phys.* **1999**, *86*, 3502–3507.
10. Lawrence, J. R.; Turnbull, G. A.; Samuel, I. D. W. Polymer Laser Fabricated by a Simple Micromolding Process. *Appl. Phys. Lett.* **2003**, *82*, 4023–4025.
11. Muller, C. D.; Falcou, A.; Reckefuss, N.; Rojahn, M.; Wiederhirn, V.; Rudati, P.; Frohne, H.; Nuyken, O.; Becker, H.; Meerholz, K. Multicolour Organic Light-Emitting Displays by Solution Processing. *Nature* **2003**, *421*, 829–833.
12. Aldred, M. P.; Contoret, A. E. A.; Farrar, S. R.; Kelly, S. M.; Mathieson, D.; O'Neill, M.; Tsoi, W. C.; Vlachos, P. A Full-Color Electroluminescent Device and Patterned Photoalignment Using Light-Emitting Liquid Crystals. *Adv. Mater.* **2005**, *17*, 1368–1372.
13. Yagi, I.; Tsukagoshi, K.; Aoyagi, Y. Direct Observation of Contact and Channel Resistance in Pentacene Four-Terminal Thin-Film Transistor Patterned by Laser Ablation Method. *Appl. Phys. Lett.* **2004**, *84*, 813–815.
14. Boiko, Y. B.; Solovjev, V. S.; Calixto, S.; Lougnot, D.-J. Dry Photopolymer Films for Computer-Generated Infrared Radiation Focusing Elements. *Appl. Opt.* **1994**, *33*, 787–793.
15. Lawrence, J. R.; O'Neill, F. T.; Sheridan, J. T. Photopolymer Holographic Recording Material. *Optik (Jena)* **2001**, *112*, 449–463.
16. Perelaer, J.; Hermans, K.; Bastiaansen, C. W. M.; Broer, D. J.;

Schubert, U. S. Photoembossed Surface Relief Structures with an Increased Aspect Ratios by Addition of a Reversible Addition-Fragmentation Chain Transfer Agent. *Adv. Mater.* **2008**, *20*, 3117–3121.
17. Trout, T. J.; Schmieg, J. J.; Gambogi, W. J.; Weber, A. M. Optical photopolymers: Design and Applications. *Adv. Mater.* **1998**, *10*, 1219–1224.
18. Hermans, K.; Tomatsu, I.; Matecki, M.; Sijbesma, R. P.; Bastiaansen, C. W. M.; Broer, D. J. Highly Efficient Surface Relief Formation *via* Photoembossing of a Supramolecular Polymer. *Macromol. Chem. Phys.* **2008**, *209*, 2094–2099.
19. van der Zande, B. M. I.; Steenbakkers, J.; Lub, J.; Leewis, C. M.; Broer, D. J. Mass Transport Phenomena during Lithographic Polymerization of Nematic Monomers Monitored with Interferometry. *J. Appl. Phys.* **2005**, *97*, 123519.
20. Kim, D. Y.; Tripathy, S. K.; Li, L.; Kumar, J. Laser-Induced Holographic Surface Relief Gratings on Nonlinear Optical Polymer Films. *Appl. Phys. Lett.* **1995**, *66*, 1166.
21. Rochon, P.; Batalla, E.; Natansohn, A. Optically Induced Surface Gratings on Azoaromatic Polymer Films. *Appl. Phys. Lett.* **1995**, *66*, 136–138.
22. Ubukata, T.; Seki, T.; Ichimura, K. Surface Relief Gratings in Host-Guest Supramolecular Materials. *Adv. Mater.* **2000**, *12*, 1675–1678.
23. Ubukata, T.; Isoshima, T.; Hara, M. Wavelength-Programmable Organic Distributed-Feedback Laser Based on a Photoassisted Polymer-Migration System. *Adv. Mater.* **2005**, *17*, 1630–1633.
24. Contoret, A. E. A.; Farrar, S. R.; O'Neill, M.; Nicholls, J. E. The Photopolymerization and Cross-Linking of Electroluminescent Liquid Crystals Containing Methacrylate and Diene Photopolymerizable End Groups for Multilayer Organic Light-Emitting Diodes. *Chem. Mater.* **2002**, *14*, 1477–1487.
25. Woon, K. L.; Aldred, M. P.; Vlachos, P.; Mehl, G. H.; Stirner, T.; Kelly, S. M.; O'Neill, M. Electronic Charge Transport in Extended Nematic Liquid Crystals. *Chem. Mater.* **2006**, *18*, 2311–2317.
26. Droege, S.; Khalifah, M. S. A.; O'Neill, M.; Thomas, H. E.; Simmonds, H. S.; Macdonald, J. E.; Aldred, M. P.; Vlachos, P.; Kitney, S. P.; Loebbert, A.; Kelly, S. M. Grazing Incidence X-ray Diffraction of a Photoaligned Nematic Semiconductor. *J. Phys. Chem. B* **2009**, *113*, 49–53.
27. Contoret, A. E. A.; Farrar, S. R.; Jackson, P. O.; Khan, S. M.; May, L.; O'Neill, M.; Nicholls, J. E.; Kelly, S. M.; Richards, G. J. Polarized Electroluminescence from an Anisotropic Nematic Network on a Noncontact Photoalignment Layer. *Adv. Mater.* **2000**, *12*, 971–974.
28. Carrasco-Orozco, M.; Tsoi, W. C.; O'Neill, M.; Aldred, M. P.; Vlachos, P.; Kelly, S. M. New Photovoltaic Concept: Liquid-Crystal Solar Cells Using a Nematic Gel Template. *Adv. Mater.* **2006**, *18*, 1754–1758.
29. Woon, K. L.; Contoret, A. E. A.; Farrar, S. R.; Liedtke, A.; O'Neill, M.; Vlachos, P.; Aldred, M. P.; Kelly, S. M. Material and Device Properties of Highly Birefringent Nematic Glasses and Polymer Networks for Organic Electroluminescence. *J. Soc. Inf. Disp.* **2006**, *14*, 557–563.
30. Dyer, P. E.; Farley, R. J.; Giedl, R. Analysis of Grating Formation with Excimer Laser Irradiated Phase Masks. *Opt. Commun.* **1995**, *115*, 327–334.
31. Woon, K. L.; Liedtke, A.; O'Neill, M.; Aldred, M. P.; Kitney, S. P.; Vlachos, P.; Bruneau, A.; Kelly, S. M. Photopolymerization Studies of a Light-Emitting Liquid Crystal with Methacrylate Reactive Groups for Electroluminescence. *Proc. SPIE—Int. Soc. Opt. Eng.* **2008**, 70500E.
32. De Gennes, P. G.; Prost, J. The Physics of Liquid Crystals; Clarendon Press: Oxford, U.K., 1993.
33. Bergmann, G.; Jackson, P. O.; Hogg, J. H. C.; Stirner, T.; O'Neill, M.; Duffy, W. L.; Kelly, S. M.; Clark, G. F. Photoinduced Changes of Surface Order in Coumarin Side-Chain Polymer Films Used for Liquid Crystal Photoalignment. *Appl. Phys. Lett.* **2005**, *87*, 061904.
34. Tsoi, W. C.; O'Neill, M.; Aldred, M. P.; Kitney, S. P.; Vlachos, P.; Kelly, S. M. Distributed Bilayer Photovoltaics Based on Nematic Liquid Crystal Polymer Networks. *Chem. Mater.* **2007**, *19*, 5475–5484.
35. Woon, K. L.; O'Neill, M.; Vlachos, P.; Aldred, M. P.; Kelly, S. M. Highly Birefringent Nematic and Chiral Nematic Liquid Crystals. *Liq. Cryst.* **2005**, *32*, 1191–1194.